Under what Conditions does (SiO)$_N$ Nucleation Occur? A Bottom-up Kinetic Modelling Evaluation

Stefan T. Bromley*[1,2]

[1]*Departament de Ciència de Materials i Química Física & Institut de Química Teòrica i Computacional (IQTCUB), Universitat de Barcelona, C/ Martí i Franquès 1, E-08028 Barcelona, Spain*

[2] *Institució Catalana de Recerca i Estudis Avançats (ICREA), 08010 Barcelona, Spain*

Juan Carlos Gomez Martin[3], John M. C. Plane*[3]

[3]*School of Chemistry, University of Leeds, Leeds, LS2 9JT, UK*

* Corresponding authors: s.bromley@ub.edu, J.M.C.Plane@leeds.ac.uk

Silicon monoxide (SiO) is a structurally complex compound exhibiting differentiated oxide-rich and silicon-rich nano-phases at length scales covering nanoclusters to the bulk. Although nano-sized and nano-segregated SiO has great technological potential (e.g. nano-silicon for optical applications) and is of enormous astronomical interest (e.g. formation of silicate cosmic dust) an accurate general description of SiO nucleation is lacking. Avoiding the deficiencies of a bulk-averaged approach typified by classical nucleation theory (CNT) we employ a bottom-up kinetic model which fully takes into account the atomistic details involved in segregation. Specifically, we derive a new low energy benchmark set of segregated (SiO)$_N$ cluster ground state candidates for $N \leq 20$ and use the accurately calculated properties of these isomers to calculate SiO nucleation rates. We thus provide a state-of-the art evaluation of the range of pressure and temperature conditions for which formation of SiO will or will not proceed. Our results, which match with available experiment, reveal significant deficiencies with CNT approaches. We employ our model to shed light on

controversial issue of circumstellar silicate dust formation showing that, at variance with the

predictions from CNT-based calculations, pure SiO nucleation under such conditions is not

viable.

Introduction

Background

The atomistic structure of bulk silicon monoxide (SiO) is particularly distinctive in that it consists of a disordered aggregation of separated nanoparticles of an insulator (silica, SiO_2) and a semiconductor (silicon) and interfaced by sub-oxide, while appearing to be unstable as a homogeneously mixed phase.[1] Control of segregation in SiO yields systems of sized controlled quantum-confined nanoparticles of silicon[2] or SiO_x [3] embedded in a SiO_2 matrix, which are of great interest for light emission applications (e.g. biomedical imaging). Recently, disproportionated SiO has also been proposed as a promising anode material for Li-ion batteries.[4,5] More generally, the Si-SiO_2 system is probably one of the most studied semiconductor-insulator systems due to its huge importance in the microelectronics industry.[6] Cluster beam experiments [7-10] and numerous computational modelling studies [11-21] have confirmed that the inherent tendency of SiO to segregate emerges in nanoclusters of only a few atoms and thereon for subsequently larger sizes strongly influences its structure and stability. The importance of understanding the formation and structure of SiO at small length scales and under a range of conditions is underlined by the technological importance of gaseous SiO and molecular $(SiO)_N$ species in the production of silicon nanowires [22] and semiconductor silicon[23] and in silane oxidation.[24] Small $(SiO)_N$ clusters have also drawn particularly strong interest from the astronomical community, where experimental and theoretical studies have investigated their potential relation to the formation of silicate dust in the interstellar medium (ISM) [25] and circumstellar environments,[26] as well as with respect to their role in interstellar chemistry.[27] However, despite the general interest in SiO and its relevance to understanding SiO_2-Si segregated systems, the bottom-up progression from

nucleating SiO monomers and clusters to a segregated nanostructured material is ill-understood.

Using a novel structure search methodology, which utilizes results from global optimization searches of nanoclusters of silicon $(Si)_N$ and silica $(SiO_2)_N$, we find new low energy segregated ground state candidates for $(SiO)_N$ clusters for N = 8-20. We then use the calculated molecular parameters and free energies of these clusters to calculate the rate coefficients for the sequential addition of SiO to $(SiO)_N$ clusters, and use these rate coefficients to predict the nucleation rate of SiO for arbitrary conditions of pressure and temperature.

Nucleation of $(SiO)_N$

Attempting to understand the stabilities and structures of small $(SiO)_N$ clusters involved in nucleation based on extrapolations from the average properties of macroscopic SiO samples (i.e. top-down approaches) will inevitably overlook the atomic/nano-scale details of segregation. Top-down approaches to SiO nucleation will thus not only introduce significant quantitative errors (as we show in detail below) but are intrinsically unable to capture qualitative features of phenomena involving nanoscale SiO. The formation of Si nanowires from the aggregation of $(SiO)_N$ species, for example, clearly involves nanoscale silica-silicon segregation and possibly fragmentation. Similar nanophase segregated particles have been proposed to possibly form from the nucleation of SiO in circumstellar environments. The subsequent fragmentation of these species into (i) nearly pure Si nanoparticles and (ii), SiO_x nanoparticles with $x \approx 2$ (i.e. silica-like), might provide a source of a carrier for a spectroscopic feature known as the extended red emission (ERE),[28,29] and could begin to provide an account of the initial stages of silicate dust growth (i.e. oxygen enrichment of SiO), respectively.

Studies using bottom-up computational modelling together with cluster beam experiments have suggested that growth and fragmentation of small silicon suboxide clusters (Si_NO_M with N = 1–17, M = N±1) could indeed occur.[19,30]

In circumstellar condensation zones where silicate dust formation is observed (1200 – 1000 K, 0.1 – 0.001 Pa), it has been argued that much of the O is locked up in SiO,[31,32] thus providing a potential monomer source for nucleation. The circumstellar nucleation of SiO monomers with respect to its possible relevance to the formation of interstellar silicate dust has been the focus of a number of top-down theoretical studies using classical nucleation theory (CNT).[33-35] Here the atomistic structures of the growing cluster isomers are not explicitly taken into account and their energetic stabilities are replaced by scaled bulk-derived average values. Typically such studies use CNT to extrapolate bulk measurements of the vapour pressure of SiO under laboratory conditions to the more extreme conditions around a star. The most recent CNT calculations [34,35] predict SiO condensation onset temperatures which are close to the lower observed bound (1000 K) for silicate dust formation environments and thus provide tentative support for the possibility of pure SiO nucleation being important for circumstellar silicate dust formation. However, it should be noted that Nuth and Ferguson[35] had to propose a concept of vibrational disequilibrium, where the SiO vibrational temperature was significantly below its kinetic temperature because of efficient radiative cooling at the low pressures of a stellar outflow, in order for the CNT nucleation rate to be fast enough.

From a molecular bottom-up perspective, for condensation processes the dominating contribution to the entropy of reaction is generally the loss of translational entropy, which is only partially compensated for by an increase in rotational and vibrational entropy. At the high temperatures around a star this huge entropy loss weighs heavily on the Gibbs free energy of reaction: $\Delta G_{rxn} = \Delta H_{rxn} - T\Delta S_{rxn}$, with $T\Delta S_{rxn}$ of the order of 200 – 300 kJ mol^{-1} for

any bimolecular addition reaction at 1000 K. Consequently, only very exothermic reactions ($\Delta H_{rxn} \ll 0$) can occur under these conditions. The heat of formation of the SiO + SiO → $(SiO)_2$ dimerization reaction has been measured to be -186 (± 12) kJ mol^{-1},[36] and consistently calculated to be within 20 kJ mol^{-1} of this value by numerous *ab initio* quantum mechanical calculations at various levels of theory.[25,26,37-39] Thus, this initial step in SiO nucleation is likely to be significantly hindered in circumstellar environments. Early efforts using calculated thermochemistry data for small $(SiO)_N$ N = 1-4 species in conjunction with reaction rate theory to study the SiO nucleation processes concluded that, indeed, the dimer formation process was the rate limiting step at 1000K for relatively high pressure conditions ($\sim 10^3 - 10^5$ Pa).[25] Herein, we employ kinetic nucleation theory together with reliable quantum chemical calculated thermochemistry data for $(SiO)_N$ N = 1-20 to provide a new benchmark evaluation of the nucleation of SiO under a variety of conditions. We specifically focus on the question of the viability of SiO nucleation under circumstellar conditions and compare our results quantitatively with the results from CNT and available experimental data. Our findings highlight the severe failings of CNT for accurately tackling this problem and unambiguously demonstrate that pure SiO nucleation is not a viable process in circumstellar environments.

Silicon sub-oxide clusters

Purely theoretical, systematic computational modelling studies have investigated the structures and properties of a range of Si_NO_M sub-oxide isomers structures of low energy isomers with N ≤ 7 using both manual searches [11-13] and global optimisation.[14] The neutral $(SiO)_N$ ground state clusters in this size range display a structural transition from simple single rings of alternating Si and O atoms (N = 2-4) to more complicated topologies at N = 5. For 5 ≤ N ≤ 7 the cluster structures display at least one Si-Si bond indicative of the initial

stages of segregation into oxygen-rich and oxygen-poor regions as found in the bulk solid. Segregation can be rationalised on structural/energetic grounds through the maximisation of the number of strong Si-O bonds (i.e. those in unstrained Si-O-Si linkages), together with the fact that silicon chemically favours to bond in a 4-fold tetrahedral manner. The optimal O:Si ratio to best satisfy both these tendencies increases from one in very small clusters and thereon increases with increasing N towards two in the bulk. For $(SiO)_N$ for N > 6 this optimal O:Si ratio is obtained using a subset of the Si atoms with the remaining Si atoms forming an Si-Si bonded sub-cluster. We note that cationic $(Si_NO_M)^+$ clusters for N = 3 - 5 and M = N, N ± 1, have also been studied by cluster beam experiments together with global optimisation calculations, whereby the latter was used to assign isomer structures to observed IR absorption spectra.[7,8] Here the tendency for Si-Si bond formation was found to start at $(SiO)_4^+$, which is also confirmed in another purely theoretical study.[15] Anionic Si_NO_M clusters for N ≤ 5 for a selection of M values have also been investigated by cluster beam experiments with the cluster structures assigned by calculations of measured electron affinities (EAs) and ionisation potentials (IPs).[9,10] The above studies generally confirm that from N = 1-7 for Si_NO_M clusters Si-Si bonds tend to start with increasing N regardless of charge state and that Si-Si bonding is particularly favoured in more oxygen deficient (i.e. N < M) sub-oxide clusters. We note that due to the matched 1:1 stoichiometry in SiO, every Si and every O atom in all lowest energy $(SiO)_N$ clusters have at least two bonds to other atoms.

        Moderate-sized Si_MO_N oxygen-rich sub-oxide clusters (i.e. where M < N, with 20 < M+N < 30 atoms) were first proposed to energetically favour structures which exhibit linked Si_2O_2 "two-rings" and Si_3O_3 "three-rings" of alternating Si and O atoms with no Si-Si bonding.[16] For N=M, however, similar sized $(SiO)_N$ clusters based on Si-Si bonded "cores" surrounded by silicon sub-oxide sheaths were first proposed to be to be lowest in energy for the size ranges N= 6–21,[17] N = 14–26,[18] and N= 5–12.[19] An alternative and considerably more

energetically stable "segregated" motif for silicon monoxide clusters was put forward for

$(SiO)_N$ N = 12-18 by Wang et al.,[20] whereby the cluster structure is formed by a small silicon

sub-cluster attached to a silicon oxide sub-cluster in a side-by-side manner. Clearly, the

experimental and computational modelling strongly confirms that small silicon sub-oxide

clusters have a strong propensity to form anisotropic structures with O-rich (i.e. silica-like)

and Si-rich (i.e. silicon-like) regions, as is known experimentally to be a feature of bulk SiO.[1]

In this study we use the knowledge gained in previous studies together with data from

global optimisation searches on fully oxidised silica $(SiO_2)_N$ clusters and $(Si)_N$ silicon cluster

species to derive new candidate ground state structures for the size range $(SiO)_N$ (N = 8-20).

Our method, described below, yields many new $(SiO)_N$ candidate global minima structures in

the range N = 8–20, the majority of which are more stable than any previously reported.

These results thus provide a new benchmark data set for the bottom-up calculation of SiO

nucleation rates.

Methodology and Results

Low energy $(SiO)_N$ cluster structures

Ideally one would like to directly search for low energy $(SiO)_N$ isomers using global

optimisation techniques on the energy landscape described by electronic structure

calculations. Unfortunately, such an approach is extremely computationally demanding and,

as far as we are aware, has only been thus far performed for two oxide cluster systems,

$(MgO)_N$ [40] and $(TiO_2)_N$,[41] with up to 32 atoms. Moreover, unlike $(SiO)_N$, these non-segregated

rather ionic systems have electrostatically driven alternating cation-anion local atomic

ordering which tends to assist global optimisation algorithms to find low energy structures.

Here, we use in-house global optimisation results for non-segregated $(SiO_2)_N$ clusters (for N = 7-13) [42-44] and published data for similar studies on small Si_N clusters (N = 3-7) [45] to assist in the derivation of low energy segregated $(SiO)_N$ clusters. We find that our approach is remarkably effective and our candidate global minima isomers for $(SiO)_N$ N = 8-20 are, in all but two cases, more energetically stable that previously reported isomers.

As noted above, $(SiO)_N$ clusters for sizes N ≥ 7 have a well-established tendency to segregate into an oxygen-rich Si_nO_N silica-like part which is linked to a Si_m part exhibiting Si-Si bonds. Moreover, with increasing cluster size, this Si_nO_N-Si_m (n+m=N) segregation appears to be most energetically favourable when occurring in an anisotropic side-by-side manner.[20] Assuming side-by-side segregation, for a cluster of composition $(SiO)_N$, we first extract low energy $(SiO_2)_x$ clusters from our global optimisation searches such that $0 < 2x-N < 6$ (i.e. which contain up to six more oxygen atoms than $(SiO)_N$). Clearly, in order to obtain a $(SiO)_N$ cluster the appropriate number of oxygen atoms must be removed from each candidate $(SiO_2)_x$ isomer. It is known that small clusters of $(SiO_2)_x$ are over-oxidised in the sense that their energetic stability with respect to their O:Si ratio is sub-optimal with respect to somewhat smaller ratios.[12,13] This can be chemically rationalised by observing that small $(SiO_2)_x$ clusters exhibit numerous oxygen atoms which reside in singly-coordinated terminating defects;[42-44] these clearly are not as strongly bound within a cluster structure as doubly coordinated Si-O-Si species. Thus, to reduce the number of oxygen atoms in a low energy $(SiO_2)_x$ isomer while improving its binding energy per oxygen atom, we remove all terminal oxygen atoms. Following the same rationale, we also produce a separate set of sub-oxide clusters where we also remove both oxygen and silicon atoms residing in energetically costly strained rings $(SiO)_R$ (R ≤ 3) [46] that are associated with a removed terminal oxygen atom.[43] In this way we produce a set of "pre-optimised" silicon sub-oxide clusters with a O:Si ratio greater than one. In order to subsequently produce a $(SiO)_N$ cluster an appropriate

number of Si atoms must be added to the cluster. Here we take a low energy Si_Y isomer [45] containing the required atom count and either: (i) place it at the position of the removed atom(s), or (ii) replace a silicon atom in a strained $(SiO)_R$ ($R \leq 3$) ring. In the former case this "heals" any under-coordinated atoms in the sub-oxide cluster. In the second scenario, the silicon cluster helps to relieve the strain in the small ring into which it is inserted.

The above procedure was followed numerous times for each $(SiO)_N$ cluster size using a range of initial low energy $(SiO_2)_x$ together with all possible suitably sized low energy silicon clusters in a wide variety of "docking" variations (e.g. position and orientation of the silicon cluster). An schematic example of this procedure is shown in Figure 1 for the case of $(SiO)_{16}$. For each $(SiO)_N$ cluster isomer produced by this method we also derive an associated candidate low energy isomer for $(SiO)_{N+1}$ by simply inserting a SiO monomeric unit into a strained $(SiO)_R$ ($R \leq 3$) ring. This latter tactic gave rise to four of our putative global minimum candidates for $(SiO)_N$, N = 12, 15, 17, 20, which, in these cases, were slightly energetically more stable than the best isomers coming directly from the original procedure. In all other cases $(SiO)_N$, N = 7, 8, 9, 10, 11, 13, 14, 16, 18, 19, the original procedure directly provided our reported putative ground states. We note that apart from the sizes N = 7, 10, all of our reported $(SiO)_N$ isomers (see figure 2) are energetically more stable than those previously reported in the literature (see comparison of binding energies in figure 3).

In order to provide some test of the effectiveness of our approach we also performed global optimisation calculations using simulated annealing (SA) with *ab initio* Langevin molecular dynamics (LMD) for the size $(SiO)_{10}$. Although our three LMD-SA runs gave rise to a number of new $(SiO)_{10}$ isomers, they did not yield any isomer lower in energy than that found by our more constructive approach. Although, this limited assesment does not mean that our reported low energy isomers are global minima, the lack of new lower energy $(SiO)_{10}$ isomers being found during the LMD-SA calculations gives us further confidence in our

results. The details of the LMD-SA calculations and all resulting isomers are included in the

Supplementary Information. Optimised atomic coordinates of all our reported $(SiO)_N$ putative

global minimum clusters can also be found in the Supplementary Information and are openly

accessible in the WASP@N cluster database [www.ucl.ac.uk/klmc/Hive] and NOMAD

repository [nomad-repository.eu/cms]).

After every $(SiO)_N$ was produced by our procedure it was subsequently optimised

using density functional theory (DFT) employing a 6-311+G(2d,p) basis set and the B3LYP

functional[47] with an ultrafine integration grid as implemented in the Gaussian 09 code.[48]

Harmonic vibrational frequencies of all cluster isomers were also evaluated at the same level

of theory and free energies (including zero point energies) under standard conditions (298.15

K / 1 atm) were evaluated in each case. The isomers with the lowest calculated free energy are

reported in Fig. 2. In table 1 we compare our calculated structures and vibrational frequencies

of the SiO monomer and the $(SiO)_2$ dimer and enthalpy of reaction of the dimerization

reaction with experimental values. The very good agreement in all cases gives us confidence

in the accuracy of our calculated quantum chemical data for use in the kinetic modelling of

the nucleation process.

Kinetics of SiO nucleation

Rate coefficients for the reactions $SiO + (SiO)_{N-1} \rightarrow (SiO)_N$ up to N = 9 were

calculated using Rice-Ramsperger-Kassel-Markus (RRKM) theory, employing a solution of

the Master Equation (ME) based on the inverse Laplace transform method.[49] For these

calculations we have assumed that any potential energy barriers involved in rearrangement to

form the most stable $(SiO)_N$ cluster are submerged with respect to the $SiO + (SiO)_{N-1}$

reactants. This assumption is supported by accurate theoretical calculations which show the

absence of a barrier for the $SiO + SiO \rightarrow (SiO)_2$ and $SiO + (SiO)_2 \rightarrow (SiO)_3$ reactions.[21]

Although a study by Pimental et al.[26] reported a modest barrier for the latter (trimerisation)

reaction, we could not verify this result and agree with the conclusion of Avramov et al.[21] that

a barrier for trimerisation does not exist. This conclusion is strongly supported by helium

droplet experiments showing that this, and similar oligomerization reactions, proceed at

temperatures as low as 0.37 K.[25] As many of our $(SiO)_N$ ground state clusters can simply be

regarded as resulting from SiO insertions into a ring in the corresponding $(SiO)_{N-1}$ isomer (and

thus analogous to the trimerisation reaction) we expect at least these steps to involve very low

or zero effective barriers. Although, strictly speaking, our calculated rate coefficients are thus

upper limits, as we show below, good agreement with the measured SiO nucleation rates over

a range of temperatures strongly supports the assumption that barriers are submerged. The

SiO – $(SiO)_{N-1}$ binding energies are listed in Table 2. The internal energies of the $(SiO)_N$

adducts were divided into a contiguous set of grains (width 30 cm^{-1}), containing a bundle of

rovibrational states calculated with statistical mechanics within the rigid-rotor harmonic

oscillator approximation.[50] The rotational constants and vibrational frequencies of the $(SiO)_N$

species, calculated at the DFT level, are listed in Table S2 in the Supplementary Information.

For dissociation to the reactants SiO + $(SiO)_{N-1}$, microcanonical rate coefficients were

determined using inverse Laplace transformation to link them directly to the capture rate

coefficient, which was estimated using the method of Georgievskii and Klippenstein.[51] The

capture rates due to dipole-dipole, dipole-induced dipole and dispersion forces were first

calculated separately (the required dipole moments, polarizabilities and ionization potentials

calculated at the DFT level are listed in Table 2). The capture rate coefficient was then set to

1.3 times the largest of the individual rate coefficients.[51] The resulting capture rate coefficient

was then assumed to be the high-pressure limiting rate coefficient, $k_{rec,\infty}$, with a $T^{1/6}$

temperature dependence.[51] The probability of collisional transfer between grains was

12

estimated using the exponential down model, where the average energy for downward transitions was set to $<\Delta E>_{down} = 150$ cm^{-1} for the case of H$_2$ as the third body.[52]

In the region of a stellar outflow where dust has been observed to form, the temperature is between 900 and 1200 K [53] and the pressure between 10^{-3} and 0.1 Pa.[54] Because of the large number of vibrational modes in the larger (SiO)$_N$ clusters, these reactions are relatively fast and well into the fall-off region between third- and second-order kinetics even at these low pressures. Hence, the calculations of k over a range of T (300 – 1200 K) and p (10^{-5} – 1 Pa) were fitted to the standard Lindemann expression containing the low- and high-pressure limiting rate coefficients, $k_{rec,0}$ and $k_{rec,\infty}$, modified by a broadening factor F_c:[55]

$$k = \frac{k_{rec,0}[M]}{1+\frac{k_{rec,0}[M]}{k_{rec,\infty}}}F_c^{\beta}, \qquad \text{where } \beta = \frac{1}{\left\{1+\left[\log_{10}(\frac{k_{rec,0}[M]}{k_{rec,\infty}})\right]^2\right\}} \qquad (I)$$

The fitted values of F_c are given in Table 3. The dissociation rate coefficients were then calculated via detailed balance through the equilibrium constants, also listed in Table 3.

Figure 4 illustrates the variation of the second-order addition rate coefficient as a function of pressure of H$_2$ (at 500 K) and temperature (at 0.01 Pa). Note that k(SiO + Si$_8$O$_8$) is essentially at the high pressure limit over this pressure range, even above 1000 K. Since the addition reactions of SiO to (SiO)$_N$ N > 8 will also therefore be at their high pressure limits, the rate coefficients for these reactions are set to their respective capture rate coefficients (Table 3).

We now consider three ways to calculate the nucleation rate (J^*) of (SiO)$_N$ particles, defined here as the rate of production of Si$_{20}$O$_{20}$ clusters: Kinetic Nucleation Theory (KNT), Classical Nucleation Theory (CNT), and a full time-resolved kinetic model. The KNT expression for J^* is given by:

$$J^* = k_{1\rightarrow2}[\text{SiO}]^2\left(1+\sum_{N=2}^{20}\frac{k_{2\rightarrow1}k_{3\rightarrow2}...k_{N\rightarrow N-1}}{(k_{2\rightarrow3}[\text{SiO}])(k_{3\rightarrow4}[\text{SiO}])...(k_{N-1\rightarrow N}[\text{SiO}])}\right)^{-1}$$

13

(II)

where $k_{m \rightarrow m+1}$ is the rate coefficient for SiO + $(SiO)_m$ (+H_2); and $k_{m \rightarrow m-1}$ is the rate coefficient for $(SiO)_m$ (+H_2) thermally dissociating to $(SiO)_{m-1}$ + SiO.[56,57] The nucleation rate $J*/[\Sigma H]$ (in s^{-1}, normalized with respect to the total H nucleus concentration i.e. $J*$ divided by $2 \times [H_2]$) is shown in Figure 5(a) as a function of p and T. The initial SiO mixing ratio is set to 7.1×10^{-5} (the cosmic abundance [58]). It has been shown previously [53] that the nucleation rate should lie in the range $10^{-22} < J_*/[\Sigma H] < 10^{-14}$ s^{-1} in order to explain the observed dust density in circumstellar shells. Inspection of Figure 5(a) shows that this condition is not met for producing SiO particles in a stellar outflow ($T > 900$ K, $P < 0.1$ Pa).

The CNT calculation of $J*$ is given by the following expression: [56]

$$J* = z \, \gamma \, S^{*} [SiO]^2 \sqrt{\frac{kT}{2 \pi \, m_{SiO}}} \, e^{-W^{*}/kT} \qquad (III)$$

where z is the Zel'dovitch factor (see below), the sticking coefficient γ is here set equal to 1 (i.e. the upper limit), S^{*} is the surface area of the critical cluster, m_{SiO} is the molecular mass of SiO, and W^{*} is the work of formation of the critical cluster, $Si_xO_x^{*}$. Figure 6 is a plot of the Gibbs free energy change for the successive addition of SiO to the $(SiO)_N$ clusters. This shows that above 600 K a significant free energy barrier develops for producing Si_6O_6 clusters, and so this is assumed to be the critical cluster size. Equation (III) can then rewritten as

$$J* = z \, \gamma \, S^{*} [SiO][Si_6O_6^{*}] \sqrt{\frac{kT}{2 \pi \, m_{SiO}}} \qquad (IV)$$

where

$$[Si_6O_6^*] = [SiO]\frac{(k_{1\to2}[SiO])(k_{2\to3}[SiO])...(k_{5\to6}[SiO])}{k_{2\to1}\,k_{3\to2}\,...\,k_{6\to5}} \tag{V}$$

The Zel'dovitch factor z for the critical cluster $Si_6O_6^*$ is given by:[59]

$$z = \left(\sum_{N=1}^{20}\frac{[Si_6O_6^*]}{[Si_NO_N]}\right)^{-1} \tag{VI}$$

The surface area S^* of $Si_6O_6^*$ can be estimated to be 1.7×10^{-14} cm^2, using the SiO bulk density of 2.18 g cm^{-3} [60] and assuming the clusters are spherical.

When applying CNT to SiO nucleation it is necessary to impose an arbitrary upper limit on the concentration of $Si_6O_6^*$ relative to SiO. This is because at temperatures below 400 K the free energy barrier is too small for the central premise of CNT – that the nucleation rate is constrained by formation of the critical cluster - to hold. In order to compare with KNT, we therefore imposed an upper limit on the critical cluster concentration: $[Si_6O_6^*] < 1 \times 10^{-10}$ [SiO]. The resulting plot of $J^*/[\Sigma H]$ versus p and T is shown in Figure 5(b), on the same scale as the KNT plot in Figure 5(a). This shows that CNT agrees reasonably well with KNT up to a pressure of 0.02 Pa, but underestimates J^* by a factor of over 1000 in the active region where $p > 0.1$ Pa.

Because the free energy surface is quite complex (Figure 6), we also used a full kinetic model to calculate J^*, in order to test KNT and CNT for this system. The coupled ordinary differential equations describing the rates of change of the concentrations of each (SiO)$_N$ N = 1-20 species were solved using a 4th-order Runge-Kutta integrator.[61] In this model, $Si_{20}O_{20}$ is defined as a sink species by setting $k_{20\to19}$ to zero. Figure 7 shows the output from full kinetic runs at $p = 0.1$ and 1 Pa (initial mixing ratio of SiO $= 7.1 \times 10^{-5}$), at a temperature of 560 K. This is the highest temperature at these pressures where nucleation is reasonably fast on a timescale of 1000 days, which is the maximum time over which dust formation occurs in a

stellar outflow once the temperature is below 1200 K.[62] If nucleation went to completion, the $Si_{20}O_{20}$ mixing ratio would be 3.6×10^{-6}. However, Figure 7(a) shows that, when $p = 0.1$ Pa, the $Si_{20}O_{20}$ mixing ratio is an order of magnitude below this value and SiO has barely decreased, even after 1000 days. In contrast, Figure 7(b) shows that at a higher pressure of 1 Pa, after 100 days the formation of $Si_{20}O_{20}$ is nearly complete and SiO has decreased by more than a factor of 10.

Note that in both cases the Si_2O_2 and Si_3O_3 clusters are relatively abundant (apart from the sink $Si_{20}O_{20}$). This behaviour is explained by inspection of the free energy surface (Figure 6), where the main barrier to nucleation at N = 6 explains the backlog of N = 2 and 3, and to a lesser extent N = 4 and 5. After the main barrier, the N = 7, 15 and 18 clusters have slightly elevated mixing ratios because relatively high free energies are required to form N = 8, 16 and 19 (Figure 6). At both pressures the nucleation rates calculated from the full kinetic integration agrees very well with KNT, but are 60 and 300 times faster than CNT at $p = 0.1$ and 1 Pa, respectively. It is not surprising that CNT does not work well for SiO nucleation. As shown in Figure 6, the free energy terrain is complex: for example, at 700 K there are positive barriers for the reactions producing the N = 4, 6, 8, 16 and 19 clusters, whereas CNT is formulated on crossing a single activation barrier.

Since circumstellar dust formation is observed at pressures below 0.1 Pa and temperatures above 1000 K,[53,62] we therefore conclude that the kinetics of SiO nucleation is much too slow under the conditions of a stellar outflow to explain dust formation above 1000 K. This conclusion was also reached by Nuth and Ferguson[35] using the CNT approach.

One experimental study with which the present model results can be compared is that of Nuth and Donn,[63] who performed SiO nucleation experiments between 700 and 950 K. They measured the critical pressure of SiO, p_c, required to generate avalanche nucleation which was defined as J^* in excess of 10^{11} cm^{-3} s^{-1}, in an H_2 atmosphere at pressures ranging

from 2600 to 6700 Pa. Figure 8 illustrates their results as a plot of p_c against T (grey line).

Also shown in the figure is our result from KNT (black line) and the full kinetic integration

model (dashed black line). Given the stated uncertainty in the experimental p_c of a factor of 4

because of the nature of molecular and/or turbulent diffusion away from the SiO source in the

reactor,[63] there is surprisingly good agreement with the theoretical models. Note that while

KNT and the full model agree extremely well between 300 and 620 K, the full model predicts

a larger p_c by up to a factor of ~4 at higher temperatures i.e. a slower rate of nucleation,

compared with KNT. This discrepancy arises because the chemical-state approximation,

which is assumed in the formulation of KNT (equation II), is less valid at higher temperatures

where the rates of unimolecular dissociation of some of the $(SiO)_N$ clusters become very fast.

A final point is that CNT fails below 600 K because of the absence of a free energy barrier.

For instance, at 400 K the p_c required to generate avalanche nucleation is predicted to be 1.4×10^{-11} torr, which is more than 6 orders of magnitude smaller than the value when kinetic

constraints are taken into account (Figure 8).

Conclusions

Based upon a new benchmark set of low energy segregated $(SiO)_N$ ground state cluster

isomers derived from joining separately globally optimised silica and silicon sub-clusters, we

perform a state-of-the-art bottom-up kinetic calculation of SiO nucleation. Through use of a

full kinetic model we evaluate the performance of KNT and CNT for the nucleating $(SiO)_N$

system. KNT is found to reproduce the nucleation rates provided by the full kinetic model for

a wide of temperatures and pressures and only tends to slightly overestimate critical pressures

for SiO nucleation at higher temperatures. Very encouragingly, the full kinetic model and, to

a slightly lesser extent KNT, match well with available experimental data regarding the

critical pressure for SiO nucleation. Conversely, CNT is not applicable at temperatures below

600 K because of the absence of a significant free energy barrier to nucleation, and at higher temperatures underestimates the nucleation rate predicted by detailed kinetics. In terms of accounting for dust formation in stellar outflows, our study clearly shows that the homogeneous nucleation of SiO is not feasible. This is because at pressures below 0.1 Pa and at temperatures above 650 K the nucleation rate $J^*/\Sigma[H]$ is less than 10^{-22} s^{-1}, which is the lower limit required to form dust on the timescale of a few 100 days.[53,62]

Acknowledgments

18

References

1.   K. Schulmeister and W. Mader, *J. Non-Cryst. Solids*, 2003, **320**, 143-150.

2.   W. Sun, C. Qian, X. S. Cui, L. Wang, M. Wei, G. Casillas, A. S. Helmy and G. A. Ozin, *Nanoscale*, 2016, **8**, 3678-3684.

3.   M. Zacharias, J. Heitmann, R. Scholz, U. Kahler, M. Schmidt and J. Bläsing, *Applied Phys. Lett.*, 2002, **71**, 2490-2492.

4.   C.-M. Park, W. Choi, Y. Hw, J.-H. Kim, G. Jeong and H.-J. Sohn, *J. Mater. Chem.*, 2010, **220** 4854-4860.

5.   J.-I. Lee and S. Park, *Nano Energy*, 2013, **2**, 146-152.

6.   D. A. Muller, T. Sorsch, S. Moccio, F. H. Baumann, K. Evans-Lutterodt and G. Timp, *Nature*, 1999, **399**, 758-761.

7.   E. Garand, D. Goebbert, G. Santambrogio, E. Janssens, P. Lievens, G. Meijer, D. M. Neumark and K. R. Asmis, *Phys. Chem. Chem. Phys.*, 2008, **10**, 1502.

8.   M. Savoca, J. Langer, D. J. Harding, D. Palagin, K. Reuter, O. Dopfer and A. Fielicke, *J. Chem. Phys.*, 2014, **141**, art. no. 104313.

9.   L.-S. Wang, J. B. Nicholas, M. Dupuis, H. Wu and S. D. Colson, *Phys. Rev. Lett.*, 1997, **78**, 4450-4453.

10.   L.-S. Wang, S. R. Desai, H. Wu and J. B. Nichloas, *Zeitschrift fur Physik D: Atoms, Molecules and Clusters*, 1997, **40**, 36-39.

11.   W. C. Lu, C. Z. Wang, V. Nguyen, M. W. Schmidt, M. S. Gordon and K. M. Ho, *J. Phys. Chem. A*, 2003, **107**, 6936-6943.

12.   Q. J. Zang, Z. M. Su, W. C. Lu, C. Z. Wang and K. M. Ho, *J. Phys. Chem. A*, 2006, **110**, 8151-8157.

13.   Q. J. Zang, Z. M. Su, W. C. Lu, C. Z. Wang and K. M. Ho, *Chem. Phys. Lett.*, 2006, **430**, 1-7.

14.   M. C. Caputo, O. Oña and M. B. Ferraro, *J. Chem. Phys.*, 2009, **130**, 134115.

15.   H.-B. Du, S.-P. Huang, A. De Sarkar, W.-J. Fan, Y. Jia and R.-Q. Zhang, *J. Phys. Chem. A*, 2014, **118**, 8893-8900.

16.   W. C. Lu, C. Z. Wang and K. M. Ho, *Chem. Phys. Lett.*, 2003, **378**, 225-231.

17.   R. Q. Zhang, M. W. Zhao and S. T. Lee, *Phys. Rev. Lett.*, 2004, **93**, art. no.: 095503.

18.   S.-X. Hu, J.-G. Yu and E. Y. Zeng, *J. Phys. Chem. A*, 2010, **114**, 10769-10774.

19.   A. C. Reber, P. A. Clayborne, J. U. Reveles, S. N. Khanna, A. W. Castleman and A. Ali, *Nano Lett.*, 2006, **6**, 1190-1195.

20.   H. Wang, J. Sun, W. C. Lu, Z. S. Li, C. C. Sun, C. Z. Wang and K. M. Ho, *J. Phys. Chem. C*, 2008, **112**, 7097-7101.

21.   P. V. Avramov, I. Adamovic, K.-M. Ho, C. Z. Wang, W. C. Lu and M. S. Gordon, *J. Phys. Chem. A*, 2005, **109**, 6294-6302.

22.   R. Q. Zhang, Y. Lifshitz and S. T. Lee, *Adv. Mater.*, 2003, **15**, 635-640.

23.   S. M. Schnurre, J. Grobner and R. Schmid-Fetzer, *J. Non-cryst. Solids*, 2004, **336**, 1-25.

24.   M. R. Zachariah and W. Tsang, *Aerosol Sci. Tech.*, 1993, **19**, 499-513.

25.   S. A. Krasnokutski, G. Rouillé, C. Jäger, F. Huisken, S. Zhukovska and T. Henning, *Astrophys. J.*, 2014, **782**, 15/11-15/10.

26.   A. S. Pimentel, F. d. C. A. Lima and A. B. F. da Silva, *J. Phys. Chem. A*, 2006, **110**, 13221-13226.

27.   M. Arakawa, R. Yamane and A. Terasaki, *J. Phys. Chem. A*, 2016, **120**, 139-144.

28.   G. Ledoux, M. Ehbrecht, O. Guillois, F. Huisken, B. Kohn, B. M. A. Laguna, I. Nenner, V. Paillard, R. Papoular, D. Porterat and C. Reynaud, *Astron. Astrophys.*, 1998, **333**, L39-L42.

29.   A. N. Witt, K. D. Gordon and D. G. Furton, *Astrophys. J.*, 1998, **501**, L111-L115.

30.   A. C. Reber, S. Paranthaman, P. A. Clayborne, S. N. Khanna and A. W. Castleman, *ACS Nano*, 2008, **2**, 1729-1737.

31.   H.-P. Gail and E. Sedlmayr, *Astron. Astrophys.*, 1986, **166**, 225-236.

32.   H.-P. Gail and E. Sedlmayr, *Faraday Disc.*, 1998, **109**, 303-319.

33.   H. P. Gail, S. Wetzel, A. Pucci and A. Tamanai, *Astron. Astrophys.*, 2013, **555**, A119.

34.   J. A. Paquette, F. T. Ferguson and J. A. Nuth, *Astrophys. J.*, 2011, **732**, art. no. 62.

35.   J. A. Nuth III and F. T. Ferguson, *Astrophys. J.*, 2006, **649**, 1178-1183.

36.   K. F. Zmbov and J. L. Margrave, *High Temp. Sci.*, 1968, **5**, 235-240.

37.   L. C. Snyder and K. Raghavachari, *J. Chem. Phys.*, 1984, **80**, 5076-5079.

38.   T. P. M. Goumans and S. T. Bromley, *Mon. Not. Roy. Astron. Soc.*, 2012, **420**, 3344–3349.

39. M. Friesen, M. Junker, A. Zumbusch and H. Schnöckel, *J. Chem. Phys.*, 1999, **111**, 7881-7888.

40. M. Haertelt, A. Fielicke, G. Meijer, K. Kwapien, M. Sierka and J. Sauer, *Phys. Chem. Chem. Phys.*, 2012, **14**, 2849-2856.

41. N. Marom, M. Kim and J. R. Chelikowsky, *Phys. Rev. Lett.*, 2012, **108**, 106801.

42. E. Flikkema and S. T. Bromley, *Chem. Phys. Lett.*, 2003, **378**, 622-629.

43. E. Flikkema and S. T. Bromley, *J. Phys. Chem. B*, 2004, **108**, 9638-9645.

44. S. T. Bromley and F. Illas, *Phys. Chem. Chem. Phys.*, 2007, **9**, 1078-1086.

45. V. E. Bazterra, O. Oña, M. C. Caputo, M. B. Ferraro, P. Fuentealba and J. C. Facelli, *Phys. Rev. A*, 2004, **69**, art. no.: 053202.

46. S. T. Bromley, I. d. P. R. Moreira, F. Illas and J. C. Wojdeł, *Phys. Rev. B*, 2006, **73**, art. no.: 134202.

47. P. J. Stephens, F. J. Devlin, C. F. Chabalowski and M. J. Frisch, *J. Phys. Chem.*, 1994, **98**, 11623-11627.

48. M. J. Frisch, G. W. Trucks, H. B. Schlegel, G. E. Scuseria, M. A. Robb, J. R. Cheeseman, G. Scalmani, V. Barone, B. Mennucci, G. A. Petersson, H. Nakatsuji, M. Caricato, X. Li, H. P. Hratchian, A. F. Izmaylov, J. Bloino, G. Zheng, J. L. Sonnenberg, M. Hada, M. Ehara, K. Toyota, R. Fukuda, J. Hasegawa, M. Ishida, T. Nakajima, Y. Honda, O. Kitao, H. Nakai, T. Vreven, J. J. A. Montgomery, J. E. Peralta, F. Ogliaro, M. Bearpark, J. J. Heyd, E. Brothers, K. N. Kudin, V. N. Staroverov, R. Kobayashi, J. Normand, K. Raghavachari, A. Rendell, J. C. Burant, S.

S. Iyengar, J. Tomasi, M. Cossi, N. Rega, J. M. Millam, M. Klene, J. E. Knox, J. B. Cross, V. Bakken, C. Adamo, J. Jaramillo, R. Gomperts, R. E. Stratmann, O. Yazyev, A. J. Austin, R. Cammi, C. Pomelli, J. W. Ochterski, R. L. Martin, K. Morokuma, V. G. Zakrzewski, G. A. Voth, P. Salvador, J. J. Dannenberg, S. Dapprich, A. D. Daniels, O. Farkas, J. B. Foresman, J. V. Ortiz, J. Cioslowski and D. J. Fox, *Gaussian 09, Revision A.1*, Gaussian, Inc., Wallingford CT, 2009.

49.   R. De Avillez Pereira, D. L. Baulch, M. J. Pilling, S. H. Robertson and G. Zeng, *J. Phys. Chem.*, 1997, **101**, 9681.

50.   D. A. McQuarrie and J. D. Simons, *Molecular Thermodynamics*, University Science Book, Sausalito, CA, 1999.

51.   Y. Georgievskii and S. J. Klippenstein, *J. Chem. Phys.*, 2005, **122**, art. no. 194103.

52.   R. G. Gilbert and S. C. Smith, *Theory of Unimolecular and Recombination Reactions*, Blackwell, Oxford, 1990.

53.   K. S. Jeong, J. M. Winters, T. Le Bertre and E. Sedlmayr, *Astronom. Astrophys.*, 2003, **407**, 191-206.

54.   J. J. Keady, D. N. B. Hall and S. T. Ridgway, *Astrophys. J.*, 1988, **326**, 832-842.

55.   S. P. Sander, J. Abbatt, J. R. Barker, J. B. Burkholder, R. R. Friedl, D. M. Golden, R. E. Huie, C. E. Kolb, M. J. Kurylo, G. K. Moortgat, V. L. Orkin and P. H. Wine, Chemical Kinetics and Photochemical Data for Use in Atmospheric Studies: Evaluation No. 17).

56.   C. Mauney, M. B. Nardelli and D. Lazzati, *Astrophys. J.*, 2015, **800**, art. no.: 30.

57.   R. Becker and W. Doring, *Annal. Phys.*, 1935, **24**, 719-752.

58.   M. Asplund, N. Grevesse, A. J. Sauval and P. Scott, in *Annual Review of Astronomy and Astrophysics*, eds. R. Blandford, J. Kormendy and E. VanDishoeck, Annual Reviews, Palo Alto, 2009, vol. 47, pp. 481-522.

59.   B. Lewis and J. C. Anderson, *Nucleation and Growth of Thin Films*, Academic Press, New York, 1978.

60.   D. R. Lide, *Handbook of Physics and Chemistry*, CRC Press, Boca Raton, FL, 2006.

61.   W. H. Press, B. P. Flannery, S. A. Tukolsky and W. T. Vetterling, *Numerical Recipes*, Cambridge University Press, Cambridge, 1986.

62.   J. M. C. Plane, *Phil. Trans. Roy. Soc. A*, 2013, **371**, art. no.: 20120335.

63.   J. A. Nuth and B. Donn, *J. Chem. Phys.*, 1982, **77**, 2639-2646.

64.   F. J. Lovas, A. G. Maki and W. B. Olson, *J. Mol. Spectr.*, 1981, **87**, 449-458.

65.   R. K. Khanna, D. D. Stranz and B. Donn, *J. Chem. Phys.*, 1981, **74**, 2108-2115.

66.   J. S. Anderson and J. S. Ogden, *J. Chem. Phys.*, 1969, **51**, 4189-4196.

67.   K. F. Zmbov, L. L. Ames and J. L. Margrave, *High Tempe. Sci.*, 1973, **5**, 235-240.

68.   J. W. Hastie, R. H. Hauge and J. L. Margrave, *Inorg. Chim. Acta.*, 1969, **3**, 601-606.

Physical Chemistry Chemical Physics

Table 1. Comparison of B3LYP/6-311+G(2d,p) calculated structural, vibrational and energetic data with experimental values. The calculated and experimental dimerization enthalphies are reported for standard conditions ($\Delta H_{298.15K}$). The calculated trimerisation reaction enthalpies are given for 0 K (i.e. reaction energy including only zero point energy corrections) to better compare with the respective experimental data taken at 0.37 K. The error in the experimental trimerisation reaction energy is taken to be 30% as estimated to be an upper bound on the uncertainty in the reported value given the approximations employed in its derivation.[25]

| N	Si-O bond length (Å)		Si-O-Si angle (°)		Vibrational frequencies (cm^{-1})		Reaction enthalpy (kJ mol^{-1})	
	Calc.	Exp.	Calc.	Exp.	Calc.	Exp.	Calc.	Exp.
1	1.5153	1.5097 [64]	-	-	1245.7	1224.4 [65]	-	-
2	1.7061	1.71 [66]	86.95	87	ω_1=232.4 ω_4=752.1 ω_5=790.8	ω_1=252 ω_4=766.3 ω_5=804.4 [65]	-193	-187 ± 13 [67] -197 ± 8 [68] -192 ± 8 [36]
3	1.6788	1.70	137.60	140	ω_3=304.2 ω_5=610.8 ω_6=610.8 ω_8=944.6	ω_3=311 ω_5=621 ω_6=630 ω_8=972.2 [65]	-231	-291 ± 87 [25]

25

Table 2. Bond energies, ionization potentials, dipole moments and polarizabilities of the $(SiO)_N$ clusters up to N = 20.

N	$\Delta H_{0\,K}(SiO + (SiO)_{N-1} \rightarrow (SiO)_N)$ / kJ mol^{-1}	IP / eV	μ_D / Debye	α / 10^{-24} cm^3
1	-	11.5	3.23	4.10
2	-188.3	9.2	0.00	8.25
3	-220.9	8.9	0.00	13.2
4	-140.6	8.3	0.00	18.0
5	-182.4	8.1	0.83	22.1
6	-148.1	7.8	2.30	25.5
7	-278.9	8.1	0.41	28.5
8	-172.1	7.1	2.03	33.9
9	-233.1	7.7	2.04	38.3
10	-272.6	7.7	1.16	43.0
11	-230.8	7.8	1.34	46.6
12	-288.1	7.8	0.98	48.6
13	-185.9	7.8	1.34	53.3
14	-257.9	8.4	0.80	58.2
15	-254.8	8.0	1.51	60.3
16	-212.8	8.0	1.17	62.6
17	-223.8	8.0	1.49	67.6
18	-229.8	8.0	2.04	72.6
19	-252.6	8.0	3.60	77.1
20	-209.9	8.0	3.88	81.9

Table 3. Low- and high-pressure limiting rate coefficients, broadening factors and equilibrium constants for the sequential addition of SiO to $(SiO)_N$ clusters in H_2, for a pressure range 10^{-4} to 0.1 pa and temperature range 300 – 1200 K. Note that formation of clusters larger than N = 9 are essentially at the high pressure limit for $p > 10^{-5}$ Pa.

	$\log_{10}(k_{rec,0}\ /\ cm^6\ molecule^{-2}\ s^{-1})$	$k_{rec,\infty}(300\ K)$ [a] $10^{-10}\ cm^3\ molecule^{-1}\ s^{-1}$	F_c	K_{eq}
SiO + SiO	$-21.75 - 3.941\ \log T + 0.1392\ \log T^2$	9.4	0.5	$4.41 \times 10^{-27}\ \exp(22436/T)$
SiO + Si_2O_2	$-7.768 - 8.868\ \log T + 0.6995\ \log T^2$	7.0	0.2	$8.44 \times 10^{-27}\ \exp(25900/T)$
SiO + Si_3O_3	$-28.02 + 9.910\ \log T - 3.235\ \log T^2$	7.7	0.2	$2.62 \times 10^{-25}\ \exp(15927/T)$
SiO + Si_4O_4	$0.4691 - 9.370\ \log T + 0.1283\ \log T^2$	8.1	0.2	$2.25 \times 10^{-28}\ \exp(21789/T)$
SiO + Si_5O_5	$-31.83 + 17.55\ \log T - 5.306\ \log T^2$	8.5	0.3	$1.34 \times 10^{-25}\ \exp(16850/T)$
SiO + Si_6O_6	$2.274 - 8.150\ \log T + 0.2383\ \log T^2$	8.7	0.2	$5.76 \times 10^{-30}\ \exp(33767/T)$
SiO + Si_7O_7	$-44.94 + 30.31\ \log T - 7.638\ \log T^2$	9.0	0.5	$5.34 \times 10^{-27}\ \exp(20131/T)$
SiO + Si_8O_8	$-72.18 + 47.71\ \log T - 9.945\ \log T^2$	9.2	0.6	$4.86 \times 10^{-28}\ \exp(27541/T)$
SiO + Si_9O_9	-	9.7	-	$1.17 \times 10^{-27}\ \exp(32460/T)$
SiO + $Si_{10}O_{10}$	-	10.0	-	$6.88 \times 10^{-28}\ \exp(27257/T)$
SiO + $Si_{11}O_{11}$	-	10.3	-	$1.06 \times 10^{-28}\ \exp(34495/T)$
SiO + $Si_{12}O_{12}$	-	10.4	-	$1.06 \times 10^{-25}\ \exp(21358/T)$
SiO + $Si_{13}O_{13}$	-	10.7	-	$2.34 \times 10^{-29}\ \exp(31001/T)$
SiO + $Si_{14}O_{14}$	-	11.1	-	$1.11 \times 10^{-26}\ \exp(29852/T)$
SiO + $Si_{15}O_{15}$	-	11.2	-	$2.17 \times 10^{-31}\ \exp(25642/T)$
SiO + $Si_{16}O_{16}$	-	11.3	-	$4.25 \times 10^{-25}\ \exp(25856/T)$
SiO + $Si_{17}O_{17}$	-	11.5	-	$1.05 \times 10^{-25}\ \exp(26605/T)$
SiO + $Si_{18}O_{18}$	-	11.8	-	$4.76 \times 10^{-35}\ \exp(31231/T)$
SiO + $Si_{19}O_{19}$	-	12.0	-	$7.42 \times 10^{-26}\ \exp(24229/T)$

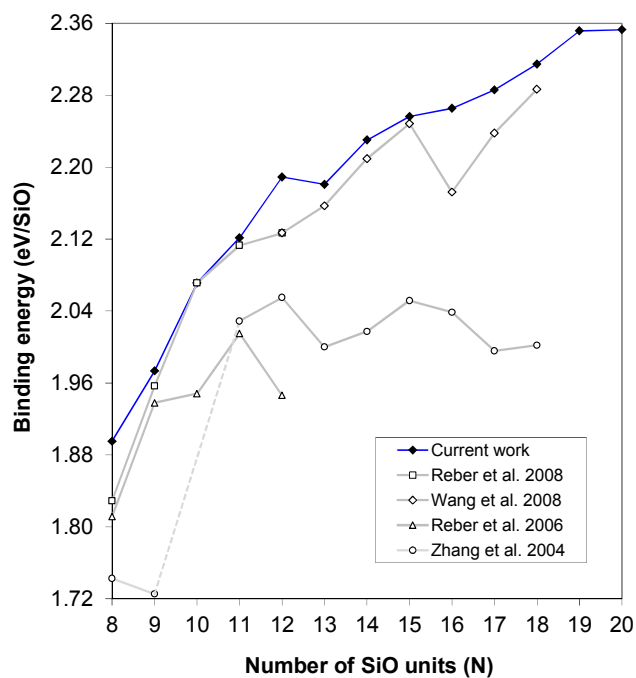[a] Temperature dependence $(T/300\ K)^{1/6}$
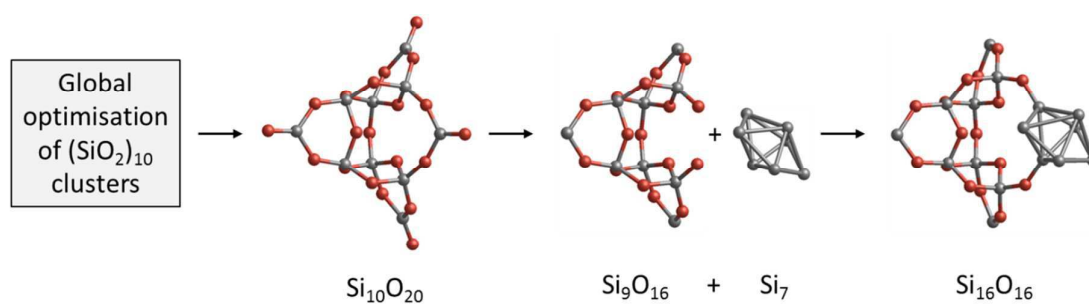
Figure 1. Schematic representation of the general procedure used to derive low energy $(SiO)_N$ isomers from joining low energy $(SiO_2)_X$ and low energy Si_Y cluster isomers, for the case $(SiO)_{16}$. Element key: Si – grey, Oxygen – red.
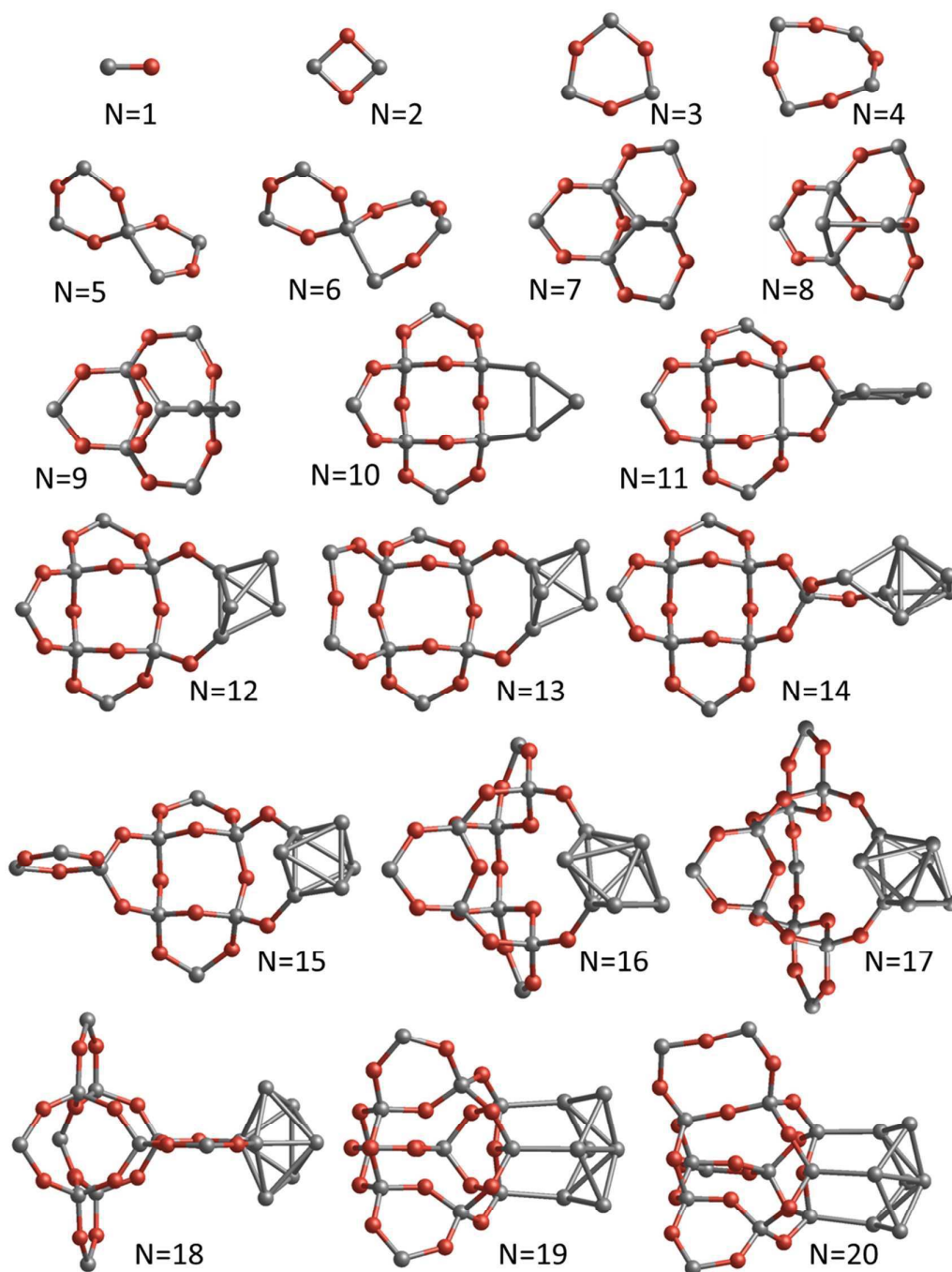
Figure 2. Candidate ground state $(SiO)_N$ cluster isomers derived in this work. Element key: Si – grey, Oxygen – red.

Figure 3. Calculated binding energies in eV per SiO unit for our $(SiO)_N$ ground state candidate clusters (see Fig. 2) as compared to previously reported $(SiO)_N$ ground state candidates in the size range N = 8 - 20.

Physical Chemistry Chemical Physics
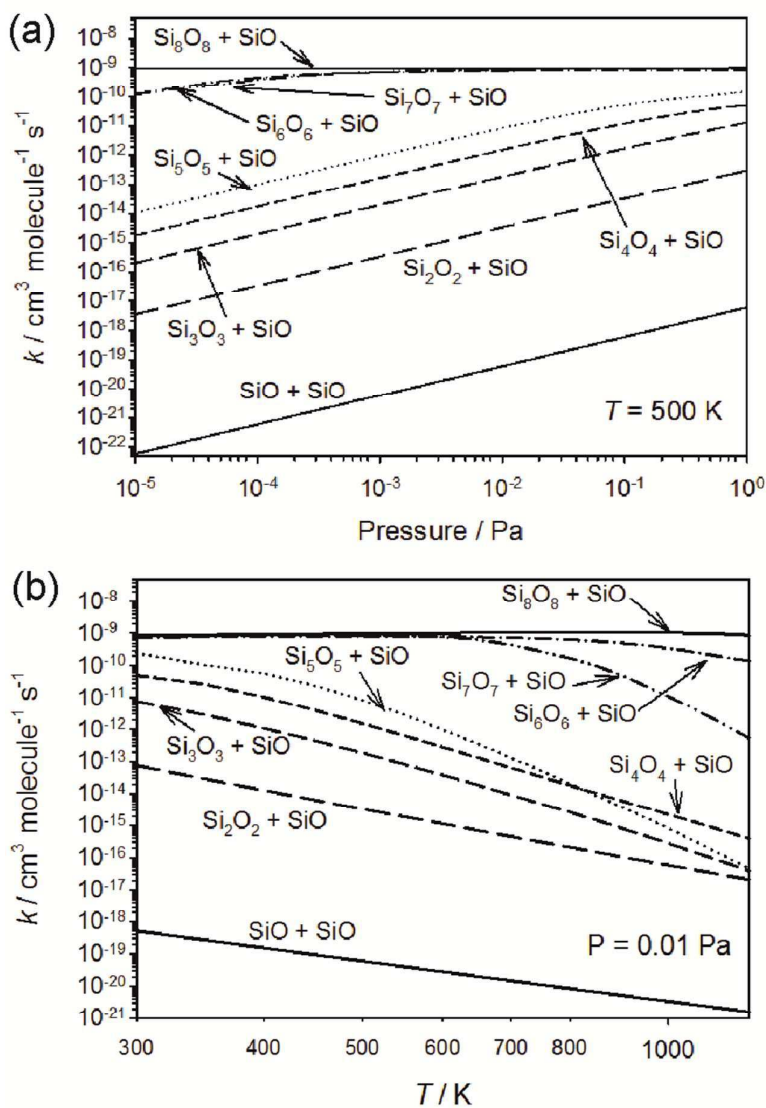
Figure 4. Calculated recombination rate coefficients for the reactions $SiO + Si_NO_N$ in H_2: (a) as a function of pressure; (b) as a function of temperature.
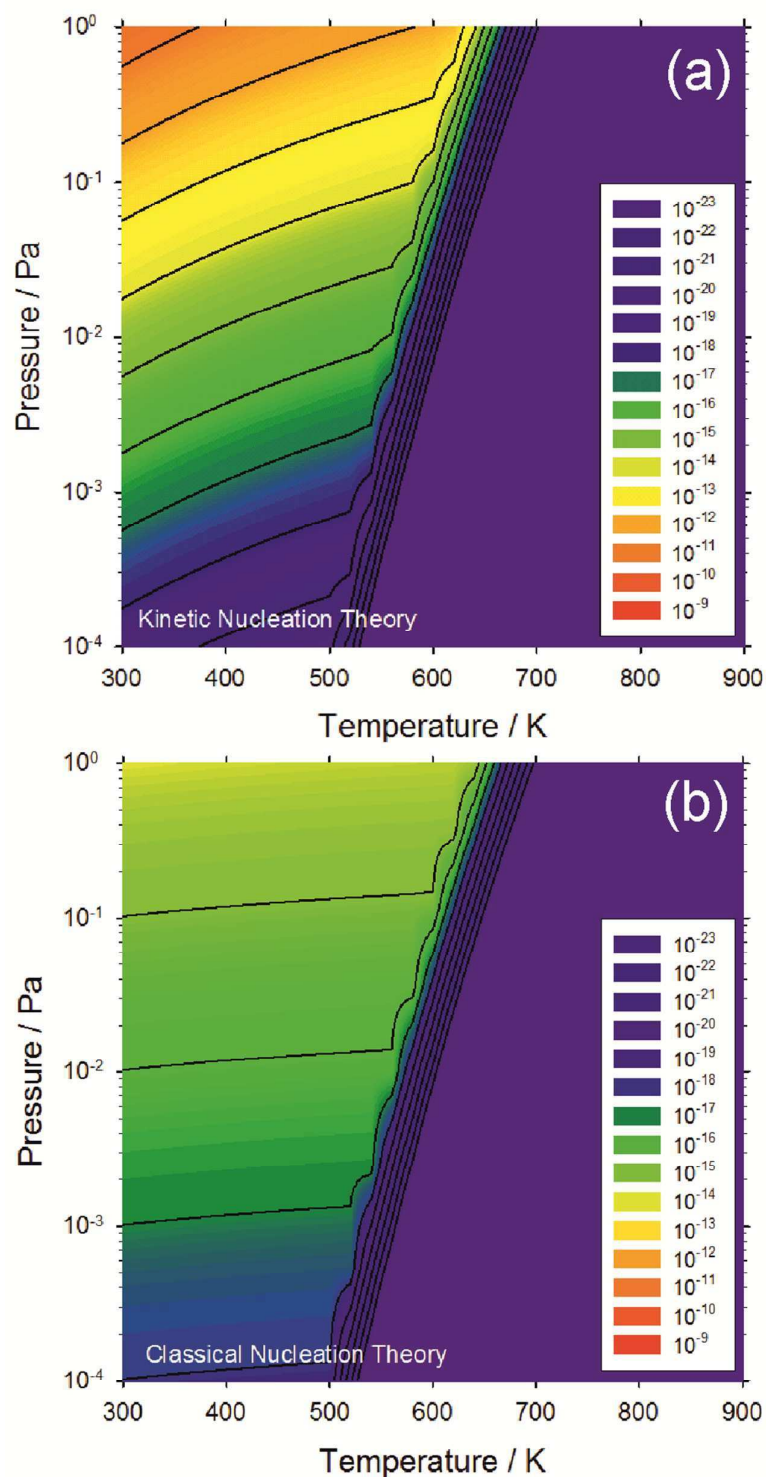
Figure 5. The nucleation rate $J^*/[\Sigma H]$ (in s^{-1}, expressed as a mixing ratio with respect to the total H nucleus concentration) of $Si_{20}O_{20}$ clusters as a function of H_2 pressure and temperature: (a) Kinetic nucleation theory; (b) Classical nucleation theory. The initial SiO mixing ratio is set to 7.1×10^{-5} (cosmic abundance).
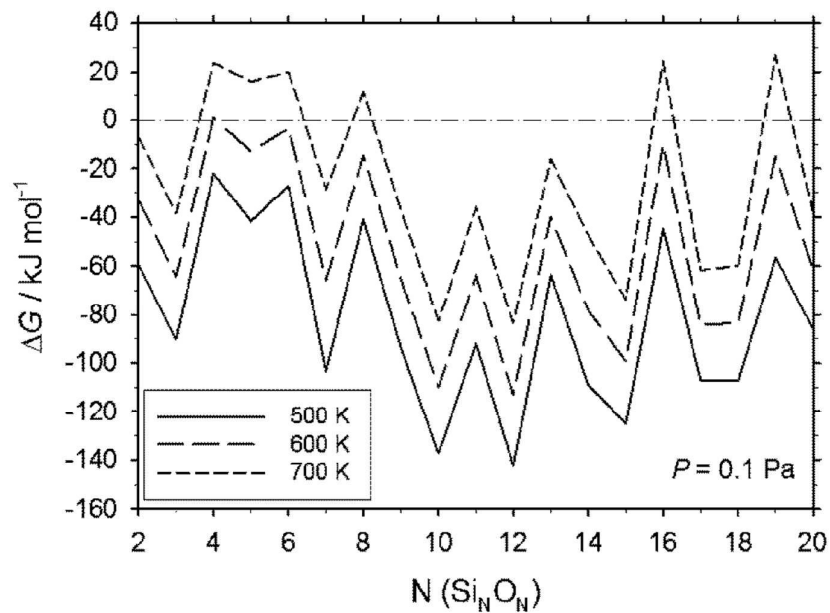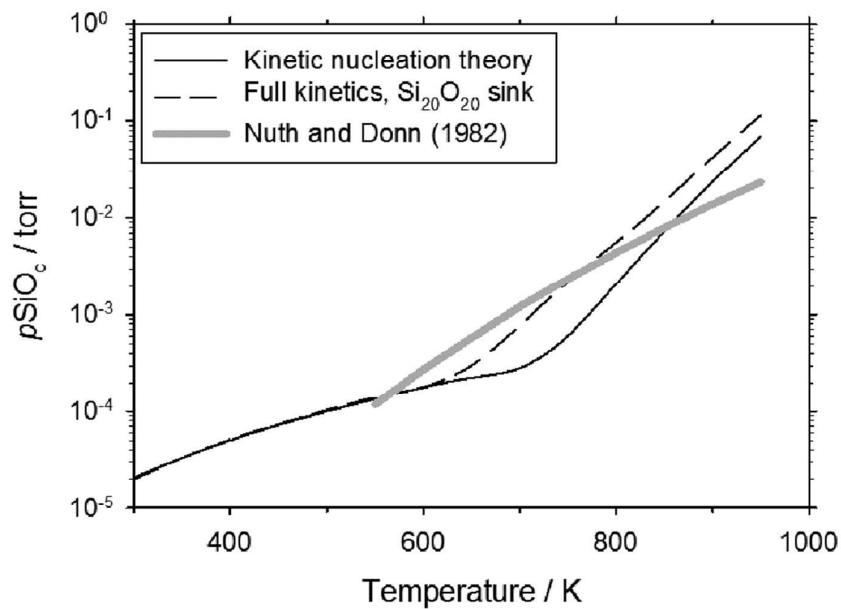
Figure 6. ΔG for the reaction $SiO + Si_{N-1}O_{N-1} + SiO \rightarrow Si_NO_N$ at a pressure of 0.1 Pa.

33
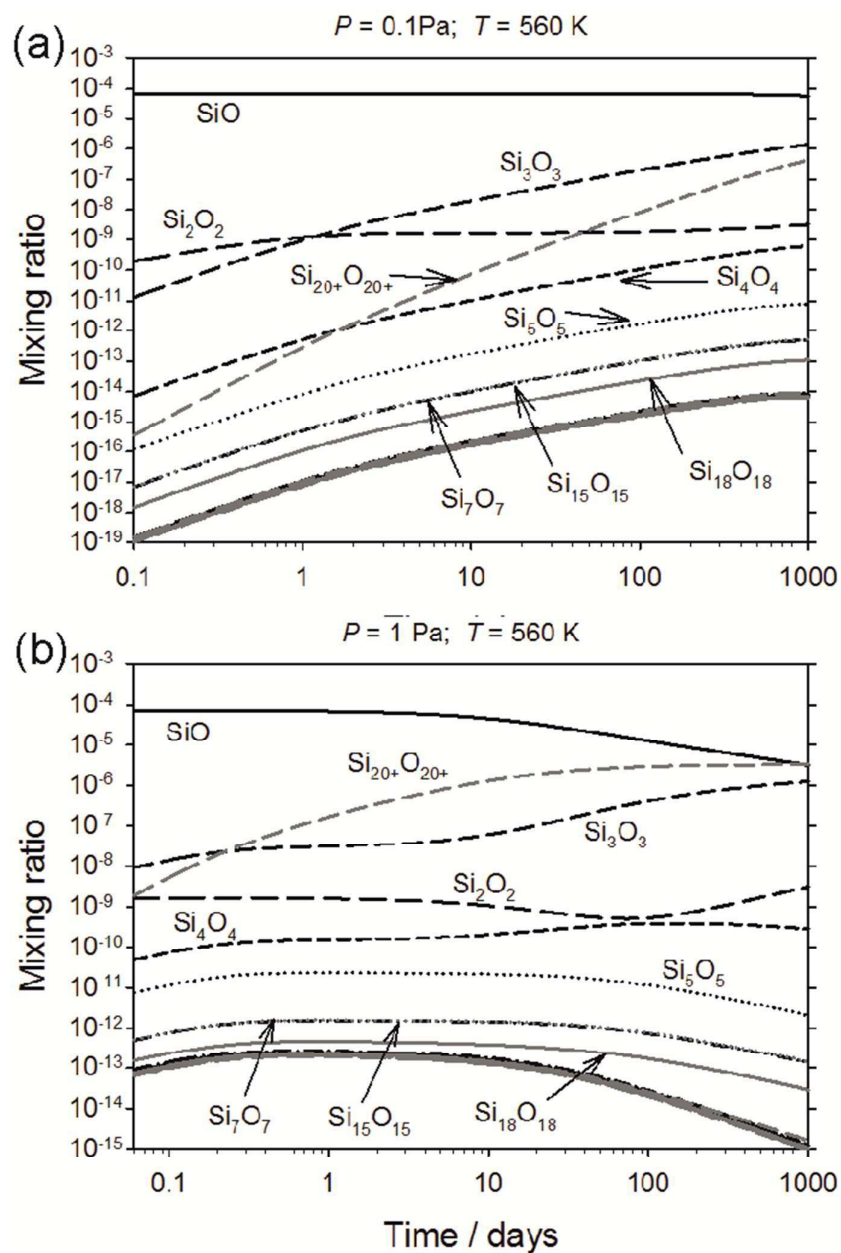
Figure 7. Full time-resolved kinetic model calculation of the evolution of $Si_N O_N$ clusters at 560 K: (a) pressure = 0.1 Pa; (b) pressure = 1.0 Pa. The initial SiO mixing ratio is set to 7.14×10^{-5} (cosmic abundance).

Figure 8.   Plot of the critical pressure for SiO nucleation pSiO$_c$ versus temperature, comparing the experimental results of Nuth and Donn.[63]

35

36